Korean J. Chem. Eng., **29**(11), 1516-1524 (2012)
DOI: 10.1007/s11814-012-0062-8

Particle size control effect on activity and selectivity of functionalized CNT-supported cobalt catalyst in Fischer-Tropsch synthesis

Ali Karimi*,, Bahram Nasernejad*,†, and Ali Morad Rashidi****

*Chemical Engineering Department, Amir Kabir University of Technology, 424 Hafez Ave., Tehran 15875-4413, Iran
**Nanotechnology Research Center, Research Institute of Petroleum Industry, Tehran, Iran
(*Received 10 March 2012 • accepted 9 May 2012*)

Abstract−The influence of cobalt particle size on catalyst performance in Fischer-Tropsch synthesis (FTS) has been investigated using functionalized carbon nanotube (CNT)-supported nano catalyst. The catalysts were synthesized by wet impregnation and special sol-gel technique. The catalysts were characterized by BET, XRD, H_2 chemisorption, TPR, and TEM. According to TEM analysis, small Co particles (3-8 nm) synthesized by sol-gel technique have very narrow particle size distributions and are mostly confined inside the CNT. The deposition of cobalt nanoparticles synthesized by sol-gel technique on the functionalized CNT shifted the reduction peaks to a low temperature, indicating higher reducibility for uniform cobalt particles. The proposed sol-gel technique increased the FTS rate from 0.62 to 0.71 g HC/gcat./h, C_5^+ selectivity increased 7% and CH_4 selectivity decreased 4%, compared to that prepared by incipient wetness impregnation. This new catalyst preparation method may offer an attractive alternative for nanoparticles synthesis with uniform, and various size distributions.

Key words: Fischer-Tropsch Synthesis, Carbon Nanotube, FTS Activity and Selectivity, Functionalization, Cobalt Particle Size

INTRODUCTION

There is a renewed interest in Fischer-Tropsch synthesis (FTS) in both academia and industry, largely as a result of the demand for clean and renewable transportation [1]. In the FTS reaction, syngas (a mixture of CO and H_2), is converted into liquid fuel via catalytic surface polymerization, which leads to a large variety of products such as paraffins, olefins, alcohols and aldehydes [1-3]. Supported cobalt catalysts are well-known for their activity and selectivity towards FTS. High chain growth probability, lower deactivation rates, low water-gas shift activity, and low costs make cobalt catalysts the best candidates for converting syngas to clean liquid fuels [4,5].

Many investigations have been carried out to study the influence of catalyst properties on FTS, including the influence of catalyst preparation techniques, to have better understanding of the structure sensitive effects in FTS catalysis [1,6-10]. A sub-category of structure-sensitive reactions regards the dependence of both catalytic activity and selectivity on catalytic metal particle size [11,12]. It is well documented that the metal particle size of the catalyst is a parameter of importance for the CO hydrogenation mechanism [1, 11,12]. Sol-gel technique for catalyst preparation enables the control of metal particle size [8,13-18]. However, it has been also shown that cobalt nanoparticles obtained by different techniques interact strongly with oxygen-carrying ceramic supports (such as Al_2O_3, SiO_2 and TiO_2). Such interactions lead to a decrease of the catalyst reduction efficiency [6,19,20]. Therefore, oxidic carriers impose serious limitations on the investigation of structure-sensitive effects in FTS catalysis because of the co-existence of incompletely reduced cobalt phase, caused by strong interaction with the oxidic carrier [2,6,19,21]. Specifically, nanoparticles are known to be more difficult to reduce on oxidic carriers. Although, it has been shown that with modifying the catalyst carrier, high reducibility can be obtained [2,6]. Moreover, previous work has shown that carbon nanotubes (CNT), when used as a cobalt catalyst support, allow a better metal dispersion control and minimize the metal phase interaction (formation of mixed compounds) with the support [2,10,22-24]. Chen et al. observed that the confinement of the Fe particles within the CNT enables a better reducibility and leads to higher rates of the CO dissociative adsorption on the metal surface [25]. Since the chemisorption of reactants is the rate determining step on FTS reaction, a cobalt particle located inside the tubes must be more active than one on the outer surface of the CNT [21-25]. Although, it is not clear until now if this phenomenon is due only because of the metal-CNT walls particular interactions.

According to previous works, the purpose of functionalization of CNT support is to increase the BET surface area and the cobalt dispersion on catalyst surface by allowing cobalt particles to go inside the CNT [22-24,26]. On the other hand by functionalization of CNT the polarity of the surface significantly increased due to the introduction of oxygen containing surface groups. Due to oxidation of defect-rich regions, the inner tubes are further opened. Furthermore, the surface groups act as sites of interaction with metal precursor [27].

It is considered that the formation of functional group on CNT surface in functionalization step not only obstructed the sintering of cobalt, but also promoted activating hydrogen or accelerated the hydrogen spill-over effect under the reduction process, contributing to realizing higher dispersion and reduction degree of these catalysts simultaneously [28].

†To whom correspondence should be addressed.
E-mail: banana@aut.ac.ir

Table 1. The composition and properties of the catalysts

Catalyst	Co (wt%)	Preparation method	XRD $d_{Co_3O_4}$ (nm)	BET (m^2/g)	Pore volume (cm^3/g)	Pore radius (nm)
CNT	--	-------	---------	255	0.73	5.82
C_1	15	Sol-gel	4.2	215	0.57	4.81
C_2	15	Sol-gel	6.4	200	0.56	5.09
C_3	15	Sol-gel	8.6	195	0.54	5.18
C_4	15	Incipient	11.1	221	0.61	6.19

This research compares the sol-gel technique and common incipient wetness impregnation method in order to control of cobalt metal particle size using functionalized CNT as a catalyst support. Formation of functional groups on CNT surface causes a higher dispersion and reduction degree, which causes the reduction peaks to shift to lower temperature. At the end of this research, the influences of cobalt particle size on the FTS Co/CNT catalysts activity and selectivity as well as the reducibility are evaluated and reported.

EXPERIMENTAL

1. Preparation and Oxidation of CNT

CNT was synthesized through methane decomposition at 900 °C over cobalt-molybdenum nanoparticles supported nanoporous magnesium oxide (Co-Mo/MgO) by a chemical vapor deposition (CVD) process [26]. The reaction of methane decomposition was conducted at atmospheric pressure with a holding time of 20-50 min. The purification procedure was as follows: A pristine CNT sample was added to an 18% HCl solution and mixed for about 16 h at ambient temperature. The resulting mixture was filtered and washed several times with distilled water until the pH of the filtrate was neutral. To achieve extra-purification, the prepared materials were dissolved in 6 M nitric acid for 3 h at 70 °C. After that, the washing step was repeated as mentioned above for the HNO_3 treatment process. The resulting cake was dried at 120 °C for 8 h, and to eliminate the amorphous carbons the temperature was increased to 400 °C for 30 min [26, 29]. The purity of the CNT was about 95%, with their diameters and lengths ranging between 10-20 nm and 5-15 μm, respectively. Functional groups such as C-OH and -COOH on CNT are commonly made by treating them in strong oxidants such as sulfuric acid (H_2SO_4) and nitric acid (HNO_3). One gram of CNT was suspended in 40 mL of a mixture of concentrated nitric acid and sulfuric acid (1 : 3 v/v) and dispersed with the aid of an ultrasonic water bath for 60 min at 60 °C. CNT was filtered from acid solution and washed with deionized water until the pH level of CNT attained to around 7. The soaked CNT was then dried in vacuum oven at 120 °C for 12 h.

2. Catalyst Preparation

The C_1-C_3 catalysts were prepared using functionalized CNT and cobalt nitrate ($Co(NO_3)_2 \cdot 6H_2O$ 99.0%, Merck), as raw materials and citric acid as complexing agent by sol-gel process from excess solution, with loadings of 15 wt% cobalt, according to the following procedure. Citric acid as complexing agent at three molar ratios of metal ion to citric acid (1, 5 and 10) was added to an aqueous solution of cobalt nitrate under vigorous stirring and heated to 83 °C in a water bath. After two minutes functionalized CNT was added to this solution. A brown gas which was NOx released from mixture due to decomposition of nitric acid present in the slurry media. This step caused the pH of solution to rise, which facilitated formation of small particle size. This procedure was followed by slow evaporating of solvent in a rotary evaporator at 83 °C, till formation of viscous gel inside the pores of CNT (it took several hours). Upon solvent evaporation a steep increase in viscosity was apparent, which inhibited redistribution of impregnated solution upon drying of the support bodies. Furthermore, a gel-like phase was formed that favored high dispersions of the active phase after full drying [16].

The control catalyst (C_4) with loadings of 15 wt% cobalt was prepared using the incipient wetness impregnation of cobalt nitrate on CNT, followed by evaporating of solvent in a rotary evaporator.

Catalysts were dried at 105 °C and the CNT supported catalysts were calcined at 450 °C for 3 h with a heating rate of 1 °C/min under argon (Ar) flow and slowly exposed to an oxygen atmosphere during the cooling step. The cobalt loading was verified by an inductively coupled plasma (ICP) AES system. The catalysts' nomenclature, compositions and properties are listed in Table 1.

3. Catalyst Characterization

The morphology of CNT support and C_1-C_4 catalyst was characterized by transmission electron microscopy (TEM). Sample specimens for TEM studies were prepared by ultrasonic dispersion of the catalysts in ethanol, and the suspensions were dropped onto a carbon-coated copper grid. TEM investigations were carried out using a Philips CM120 (100 kV) transmission electron microscope equipped with a NARON energy-dispersive spectrometer with a germanium detector.

The surface area, pore volume, and average pore radius of the CNT and C_1-C_4 catalysts were measured by an ASAP-2010 system from Micromeritics. The samples were degassed at 200 °C for 4 h under 50 mTorr vacuum and their BET area, pore volume, and average pore radius were determined.

XRD measurements of the CNT and calcined C_1-C_4 catalysts were conducted with a Philips PW1840 X-ray diffractometer with monochromatized Cu/Kα radiation. Using the Scherrer equation, the average size of the Co_3O_4 crystallites in the calcined catalysts was estimated from the line broadening of a Co_3O_4 at 2θ of 36.88°. A K factor of 0.89 was used in the Scherrer formula. The Co_3O_4 particle size was converted to the corresponding cobalt metal particle size according to the relative molar volumes of metallic cobalt and Co_3O_4. The resulting conversion factor for the diameter of a given Co_3O_4 particle $d_{Co_3O_4}$ being reduced to metallic cobalt is [11]:

$$d_{Co^0}\,(\text{nm}) = 0.75 \times d_{Co_3O_4} \quad (1)$$

Temperature programmed reduction (TPR) spectra of the C_1-C_4 catalysts were recorded using a Micromeritics TPD-TPR 2900 system, equipped with a thermal conductivity detector. The catalyst sam-

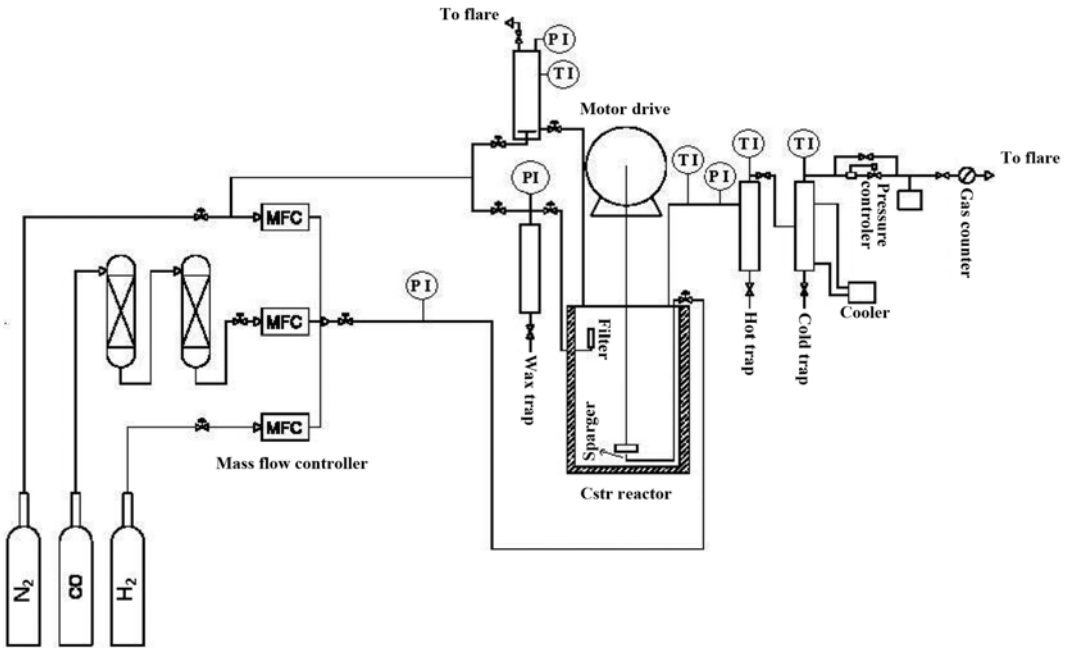

Fig. 1. Experimental setup.

ples were first purged in a flow of argon at 400 °C to remove traces of water and then cooled to 40 °C. The TPR of 50 mg of each sample was performed using 5% hydrogen in argon gas mixture with a flow rate of 40 cm^3/min. The samples were heated from 40 to 900 °C with a heating rate of 10 °C/min.

The amount of chemisorbed hydrogen (H_2) on the catalysts was measured using the Micromeritics TPD-TPR 2900 system. 0.25 g of the calcined catalyst was reduced under H_2 flow at 400 °C for 20 h and then cooled to 70 °C, always under H_2 flow. Then the flow was switched to Ar at the same temperature; this step, used to remove the physisorbed H_2, lasted for about 30 minutes. The subsequent temperature programmed desorption (TPD) of the samples was obtained by increasing the temperature of the samples, at a ramp rate of 20 °C/min, to 400 °C under Ar flow. The resulting TPD spectra were used to determine the cobalt dispersion and its surface average crystallite size. The % dispersion and particle diameter are calculated by the equations below [21].

$$\text{Calibration value (1 gas/area unit)} = \frac{\text{Loop volume} \times \%\ \text{analytical gas}}{\text{mean calibration area} \times 100} \quad (2)$$

$$\text{H}_2\ \text{uptake(moles/g}_{cat}) = \frac{\text{analytical area from TPD} \times \text{mole of H}_2\ \text{from calibration}}{\text{mean calibration area}} \quad (3)$$

$$\%\ \text{Dispersion} = \frac{\text{H}_2\ \text{uptake} \times \text{atomic weight} \times \text{stoichiometry}}{\%\ \text{metal}} = \frac{\text{number of Co atoms on surface}}{\text{number of Co atoms in sample}} \times 100 \quad (4)$$

$$\text{Diameter} = \frac{6000}{\text{density} \times \text{maximum area} \times \text{dispersion}} \times 100 \quad (5)$$

4. Catalyst Activity Test

The catalysts were evaluated in terms of their FTS activity (g HC produced/g cat./h) and selectivity (the percentage of the converted CO that appears as a hydrocarbon product) in a continuous stirred tank reactor (CSTR) as shown in Fig. 1. The volume of the CSTR was totally 1 liter. Prior to the activity tests, the catalyst activation was conducted according to the following procedure. The catalyst (10 g) with 4-6 μm size was placed in the CSTR and pure hydrogen was introduced at a flow rate of 60 NL/h. The reactor temperature was increased from room temperature to 400 °C at a rate of 1 °C/min, maintained at this activation condition for 24 h, and the catalyst was reduced in situ. After the activation period, the reactor temperature was decreased to 120 °C. Pure melted C_{28} paraffin wax was used as start-up media. C_{28} paraffin wax was degassed at degasser vessel with nitrogen at 120 °C for 1 h and transferred to the CSTR to mix with catalyst. Then the reactor temperature was increased to 180 °C under flowing hydrogen. Separate Brooks 5850 mass flow controllers were used to add H_2 and CO at the desired rate to a mixing vessel that was preceded by a lead oxide-alumina containing vessel to remove carbonyls before entering the reactor.

The mixed gases entered through a dip tube to the bottom of the CSTR below the stirrer. The CSTR was operated at 750 rpm. The temperature of the reactor was controlled via a PID temperature controller. Synthesis gas with a flow rate of 90 NL/h (H_2/CO ratio of 2) was introduced and the reactor pressure was increased to 2.5 MPa. The reactor temperature was then increased to 220 °C at a rate of 1 °C/min. Products were continuously removed from the vapor and passed through two traps, one maintained at 100 °C (hot trap) and the other at 0 °C (cold trap). The uncondensed vapor stream was reduced to atmospheric pressure through a pressure letdown valve. The flow was measured with a bubble-meter and composition of outlet gas quantified using a gas chromatograph (Varian CP-3800) equipped with TCD and FID detectors. The CO, CO_2, N_2, and O_2 were analyzed through two packed column in series (Molecular sieve13x CP 81025 with 2 m length, and 3 mm OD, and Hayesep Q CP1069 with 4 m length, and 3 mm OD) connected to TCD de-

tector. The C_1-C_5 hydrocarbons were analyzed via a capillary column (CP fused silica with 25 m×0.25 mm×0.2 μm film thickness) connected to FID detector. Hydrogen was analyzed through Shimadzu, GC PTF 4C, equipped with TCD detector and two column in series (Propack-Q with 2 m length, and 3 mm OD for CO_2, C_2H_4 and C_2H_6 separation and molecular sieve-5A with 2 m length, and 3 mmOD for CO, N_2, CH_4 and O_2 separation), which were connected to each other via a three-way valve.

The accumulated reactor liquid wax products were removed every 12 h by passing through a 2 μm sintered metal filter located above the liquid level in the CSTR. Also, the contents of hot and cold traps were removed every 12 h, the hydrocarbon and water fractions separated, and the collected liquid (Including hydrocarbons and oxygenates) were analyzed offline with Varian CP-3800 gas chromatograph equipped with capillary column (TM DH fused silica capillary column, PETRO COL 100 m×0.25 mm×0.5 μm film thickness) connected to FID detector. Both total mass and atomic material balances were performed with the consideration that a run could be accepted for further analysis if the carbon material balance closed between 97 and 103%. This criterion was adopted since compounds containing carbon and hydrogen may accumulate in the reactor, in the form of high molecular weight hydrocarbons.

The conversion percentage of CO based on the fraction of CO forming carbon-containing products per weight of catalyst (g) was calculated according to below equation:

$$\text{CO conversion} = \frac{F_{in} \times M_{CO,in} - F_{out} \times M_{CO,out}}{F_{in} \times M_{CO,in}} \times 100 \quad (6)$$

Where F_{in}, $M_{CO,in}$ and F_{out}, $M_{CO,out}$ are the molar flow, the mole percentage of CO in the syngas feed and product gas, respectively.

FTS rate (g HC/gcat./h) is equal to weight of hydrocarbons (g) produced in the reaction and defined as:

$$\text{FTS rate} = \sum F_{out} \times M_i \times MW_i / \text{g of catalyst} \quad (7)$$

Where M_i and MW_i are the mole percentage and molecular weight of product i, respectively.

The selectivity of product i (the percentage of the converted CO that appears as a given product i) is based on the total number of carbon atoms in the product and therefore is defined as:

$$\text{Selectivity of product i} = \frac{n_i \times M_i}{\sum n_i \times M_i} \times 100 \quad (8)$$

n_i is the the number of carbon atoms in product i

The C_5^+ selectivity is the total selectivity of C_5 and higher molecular weight of hydrocarbons.

According to chromatogram of GC analysis, the olefin/paraffin ratio of hydrocarbons, defined as:

$$\text{Olefin/Paraffinratioof producti (i}\geq 2) = \frac{\text{Molar sum of olefin isomers of product i}}{\text{Molar sum of paraffin isomers of product i}} \quad (9)$$

RESULTS AND DISCUSSION

1. CNT Characterization

The produced CNT was purified by acid washing and drying steps, characterized by different methods. Fig. 2 shows the SEM and TEM configuration of the as-grown CNT prepared by CVD method [24,

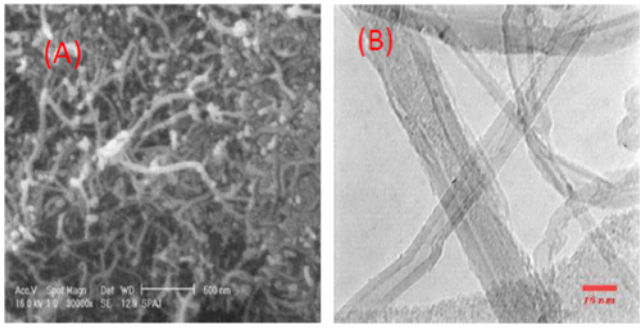

Fig. 2. (A) SEM image of CNT, (B) TEM image of CNT.

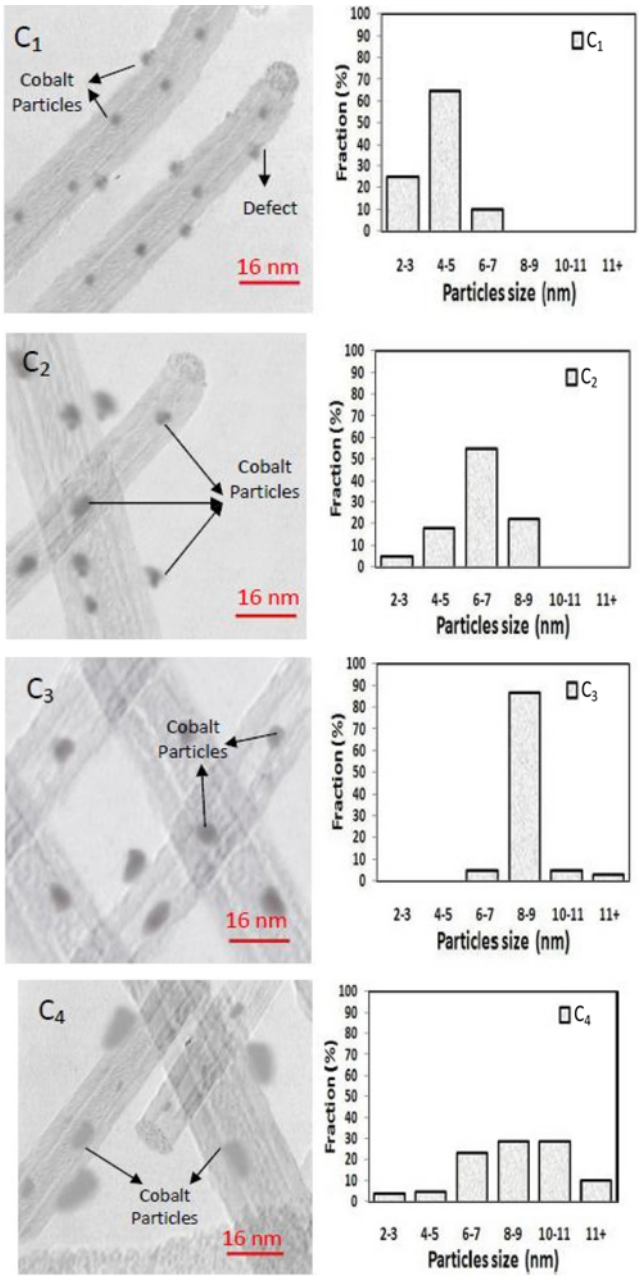

Fig. 3. TEM images of the calcined C_1-C_4 catalysts.

26].

2. Catalysts Characterization

The TEM images of the catalysts made by the sol-gel technique are shown in Fig. 3. TEM images demonstrate the uniformity of the particles made by sol-gel technique and show the particles that are inside and outside the CNT. Due to functionalization of CNT support, BET surface area and the cobalt dispersion on catalyst surface increased and cobalt particles interacted with inner walls of the CNT [22-24,26]. The C_1 and C_2 catalyst particles were both dispersed mostly inside the tube walls. For the C_3 (8-9 nm) catalyst, the percentage of the particles lying at the outer surface of the CNT walls is higher compared to the other catalysts prepared by sol-gel technique. Indeed, the narrow inner diameter of the CNT channels (9-10 nm) restricted the insertion of particles in sizes close to the channel diameter. Similar to previous works and as shown the TEM images of the C_4 catalyst made by the incipient wetness impregnation route, the smaller cobalt particles are lying inside the CNT channels and the larger particles on the outside. CNT channels have restricted the growth of the particles inside the tubes from 4 to 8 nm. Almost all particles of sizes 10 nm and over are lying on the outer surface of the CNT walls.

Also, Fig. 3 shows the cobalt particle size distribution, which is determined using the population of the total cobalt particles of each C_1, C_2, C_3 and C_4 catalysts based on data taken from different TEM images. This figure shows that sol-gel technique enables to control a narrow nanoparticle size distribution on functionalized CNT as nano catalyst support, with different molar ratio of metal ion to citric acid as a complexing agent. Indeed, these data and TPR results, which will come in the following paragraph of this article, confirm each other. According to Fig. 3, C_3 catalyst is showing narrow and uniform particle size distribution compared to C_1 and C_2 catalysts. Also, it can be seen that the average particle size for the catalyst prepared by incipient wetness impregnation method (C_4) is 6-11 nm and over. This result is in accordance with previous work [21-23].

Results of the surface area measurements in Table 1 show that the BET surface area of C_1, C_2, and C_3 catalysts decreases from 215 to 200 and 195 m^2/g, respectively. The pore volumes of different catalysts prepared by sol-gel technique remain at 0.54-0.57 cm^3/g. The lower BET surface area and pore volume of the C_1, C_2, and C_3 catalysts are comparable to the values obtained for pure CNT (255 m^2/g, 0.73 cm^3/g), indicating some pore blockage due to cobalt loading on the support. The pore volume of the C_4 is higher than the catalyst prepared by sol-gel technique (0.61 cm^3/g), indicating less pore blockage. According to the TEM pictures of the catalysts prepared by sol-gel technique, most of the small cobalt particles (<9 nm) are inside the tubes, especially for the C_1 catalyst, which in turn leads to a better interaction with the intern electron deficient walls of the CNT, but in C_4 the cobalt particles extensively interact with outer wall of CNT, an exterior electron enriched surface.

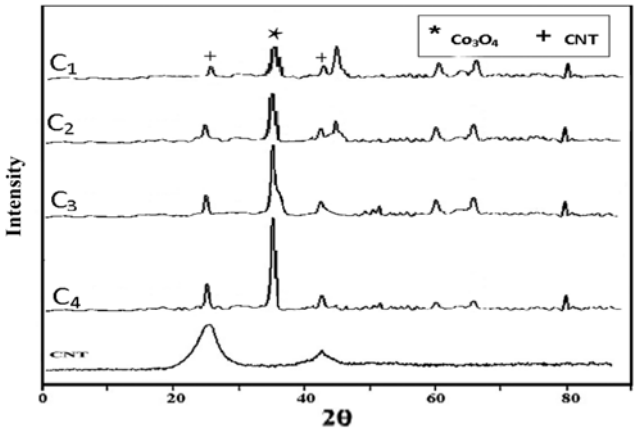

Fig. 4. XRD patterns of CNT and calcined C_1-C_4 catalysts.

XRD patterns of the calcined catalysts are shown in Fig. 4. In the XRD spectra the peaks at 2θ values of 25° and 43° correspond to the CNT support, while the other peaks in the spectra of the catalysts are related to different crystal planes of Co_3O_4 [27]. The peak at 2θ value of 36.8° is the most intense one of Co_3O_4 in XRD spectra of all catalysts. Minor peaks were also observed at 44°, and 52° for the catalysts, which correlates with a cubic cobalt structure [5]. This structure has no influence on the product selectivity [5]. Table 1 shows the average Co_3O_4 particle size of the catalysts calculated from XRD spectra using the Scherrer equation at 2θ value of 36.8° [30]. The average Co_3O_4 cluster size was determined after calcinations for the C_1, C_2, C_3 and C_4 as approximately 4.2, 6.4, 8.6 and 11.1 nm, corresponding to 3.2, 4.8, 6.4 and 8.3 nm when reduced to metal, respectively. This agrees reasonably well with the cobalt particle diameter obtained with the H_2 chemisorption results (Table 2). As shown in Table 1, the average particle sizes of Co_3O_4 are linearly correlated with the molar ratio of metal ion to citric acid as complexing agent, used during the sol-gel catalyst preparation route; the latter is also confirmed by TEM pictures of the C_1, C_2, and C_3 (Fig. 3). Increasing complexing agent concentration prevents the agglomeration of particles; the dispersion of cobalt particles increases and the smaller particles form [14].

The reducibility of the catalysts in H_2 atmosphere was determined by TPR experiments. The TPR spectra of the calcined C_1, C_2, C_3 and C_4 are shown in Fig. 5, and the specific reduction temperatures are presented in Table 2. The low temperature peak (300-380 °C) is typically assigned to reduction of Co_3O_4 to CoO, although a fraction of the peak likely comprises the reduction of the larger, bulk-like CoO species to Co^o [11,31,32]. The second broad peak is assigned to reduction of small CoO to Co^o species, which also includes the

Table 2. TPR and TPD results

Catalyst	First TPR peak (°C)	Second TPR peak (°C)	Reducibility ratio	μ mole H_2 desorbed/g cat.	% Dispersion	d_{Co^o} (nm)
C1	295	430	1.10	893.66	27.63	3.4
C2	305	425	1.17	586.40	18.13	4.2
C3	312	408	1.44	436.32	13.49	5.6
C4	370	450	1	341.23	11.98	7.2

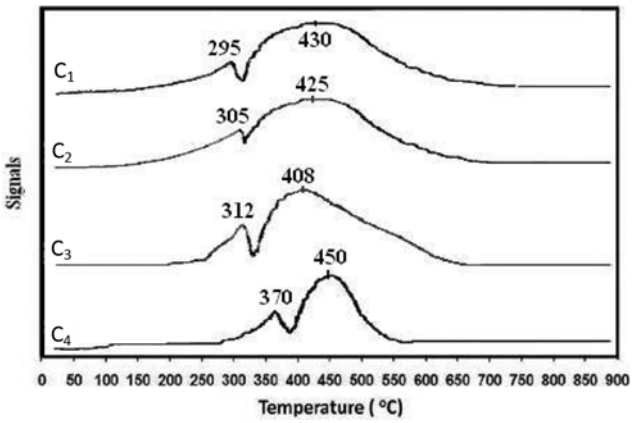

Fig. 5. TPR patterns of the calcined C_1-C_4 catalysts from 40 to 900 °C.

reduction of cobalt species that interact with the support.

According to Fig. 5, the deposition of cobalt nanoparticles synthesized by sol-gel technique on the functionalized CNT shifts the reduction peaks to a lower temperature compared to the catalyst prepared by common impregnation method on CNT, indicating higher reducibility for uniform cobalt particles produced in this special method. Interestingly, the reduction temperature of the first peak also decreases with decreasing cobalt particle size from 9 to 3 nm.

According to the TEM pictures of the catalysts prepared by sol-gel technique, most of the small particles (<9 nm) are inside the tubes, especially for the C_1 catalyst, which in turn leads to a better interaction with the intern electron deficient walls of the functionalized CNT and favors the reduction of Co_3O_4 species [24,25,28]. As shown in Fig. 5, for the C_1, C_2, and C_3 catalysts, by decreasing the cobalt particle size the second reduction peak shifts to higher temperatures and the broad shoulder of the second TPR peak becomes larger, suggesting more difficult reduction process for CoO species with 3-4 nm cobalt particles. Indeed, the degree of interaction with the metal phase and the support varies with the cobalt particles size, as larger CoO particles are reduced more easily than smaller CoO particles [1,20,23].

Table 2 also shows the reducibility ratio of all catalysts. The reducibility ratio was correlated with the amount of H_2 consumed (area under the peaks) for each part of the reduction steps (Co_3O_4 to CoO and CoO to Co^o). Thus, to have a better understanding of the compared reducibility of the catalysts, the areas under the TPR peaks were divided into two parts and were calculated by integration. The areas of the peaks are proportional to the amount of H_2 consumption. The first part is defined from 25 to 450 °C, and the second part is defined from 450 to 800 °C. The results show for C_1, C_2, C_3 catalysts, that with increasing the cobalt particle size the ratio of H_2 consumption of part one (25 to 450 °C) to the H_2 consumption of part two (450 to 800 °C) increased. This confirms that by increasing the cobalt particle size, the reduction temperature for the species that need to be reduced at high temperatures, decreases and suggests an easier reduction for larger cobalt particles. Also, the reducibility ratios of catalysts prepared by sol-gel technique are higher than the catalyst C_4, prepared by common impregnation method, which shows higher reducibility for uniform cobalt particles. These TPR results confirm the data taken from TEM images.

To conclude, uniformity of nanoparticles synthesized by sol-gel, as well as confined inside the functionalized CNT improved the reduction steps of the catalysts. Thus, particles within the functionalized CNT are easily reduced because of the confinement phenomenon for the first reduction step, but the reducibility is still more influenced by the particle size for the second step of reduction. Therefore, the confinement of Co particles in the functionalized CNT channels allowed high catalyst reducibility, which does not normally occur with nanoparticles supported on other common carriers [6,18, 25,33].

As shown in Fig. 5, there is no significant evidence of formation of metal-support compounds on the catalyst surface due to the absence of significant reduction peaks above 500 °C. Tavasoli et al., as well as Martinez et al., have noted that reduction peak present at temperatures above 530 °C with oxidic carrier shows formation of cobalt species that are difficult to reduce (oxide compounds). CNT as an inert support for cobalt catalyst do not show any peak related to formation of metal-support compounds as compared to Co/γ-Al_2O_3 catalysts, suggesting an easier reduction process with CNT than with oxidic carriers [2,21,24].

The results of the temperature programmed desorption (TPD) of the C_1, C_2, C_3 and C_4 catalysts are also given in Table 2. This table shows that in case of C_1, C_2, C_3 catalysts, the hydrogen chemisorption (H_2 uptake) decreases with increasing the cobalt particle sizes up to 9 nm in accordance with the % dispersion of the cobalt particles. Thus, increasing the cobalt particle size decreases the % dispersion from 27.63 to 13.49% (see Table 2).

The H_2 uptake of the C_3 catalyst is higher than the C_4 catalyst. It has been shown that narrow particle size distributions are more efficient for H_2 chemisorption than particle size distributions obtained with the impregnation method [6]. Moreover, Bezemer et al. observed that H_2 uptake is directly related to particle size for particles less than 10 nm, a trend which levels-off for bigger particles [1].

3. Activity and Product Selectivity for FTS

The catalytic activity and product selectivity data have been calculated for runs showing catalyst stability within the first 120 h of operation and have been reproduced twice to confirm the results' reproducibility. Fig. 6 shows the influence of cobalt particles size on FTS rate (g HC produced/gcat./h) and CO conversion. In case of C_1, C_2 and C_3 catalysts the particles are mostly inside the CNT walls, and preliminary results show that the FTS activity decreases

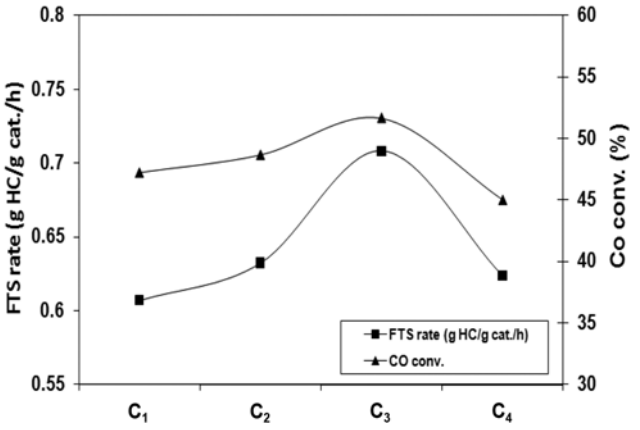

Fig. 6. CO conversion FTS rate of the calcined C_1-C_4 catalysts.

as the size of the CNT supported cobalt particles is decreased. It appears that the particles located inside the CNT and the particle size itself influences the FTS activity [1,20,25].

The comparative results of %CO conversion, FTS rate (g HC produced/gcat./h) for C_3 and C_4 catalysts are presented in Fig. 6. The proposed sol-gel technique increased the FTS rate and %CO conversion from 0.62 to 0.71 g HC/gcat./h and %45 to %52, respectively, C_5^+ selectivity increased 7% and CH_4 selectivity decreased 4%, compared to that prepared by common incipient wetness impregnation. C_4 catalyst is characterized by different particle size distribution, compared to C_3 catalyst, showing narrow and uniform particle size distribution, which particles are mostly inside the tubes. Because of uniformity, the cobalt sites produced inside the functionalized CNT (here by sol-gel technique) are more stable, and more catalytically active than the ones produced by incipient wetness impregnation [24,25,28]. Chen et al. observed that particle size is not the only property to have an effect on the FTS activity [25]. Martinez et al. observed that a narrow particle size distribution enhances the turn over frequency (TOF) of the FTS catalysts, which in turn leads to a better conversion of the reactants as well as an increase in the FTS rate [6]. Thus, improvement of the uniformity of the catalyst particles supported on functionalized CNT leads to a better CO conversion, stability of the products and the FTS activity and selectivity. These results reveal that FTS activity of the catalysts is strongly dependent on the size distribution of the cobalt cluster, and the particle's confinement within functionalized CNT may be more important than the particle size effect for the FTS activity.

Fig. 7 clearly shows that the CH_4 selectivity is reduced with increasing cobalt cluster size. Compared to C_1 and C_2 catalysts, the C_3 catalyst showed lower selectivity to methane. The lower production rate of CH_4 for the cobalt catalyst could be due to the effective participation of olefins in the carbon-carbon chain propagation. Thus, on the C_3 catalyst, α-olefins of the type R-CH=CH_2 can compete with carbon monoxide and heavier olefins for re-adsorption and chain initiation [10]. Moving upward with average particle sizes from 3 to 11 nm resulted in 5% improvement in the C_5^+ selectivity of the catalyst. According to Fig. 7, at the range of 3-4 nm the C_5^+ selectivity is already 84%. This result reveals that the dissociative adsorption of CO and chain growth probability (α-olefins re-adsorption) on the propagation step is efficient even with 3-4 nm particles due to beneficial electronic properties of the internal CNT walls [10]. The selectivity for C_5^+ products on the functionalized CNT supported cobalt catalyst, synthesized by sol-gel method, is still higher for larger particles (8-9 nm). According to Chen et al. the particle sintering is effectively prevented inside CNT due to spatial restriction of the CNT channels which stabilized the activity and selectivity of the cobalt particles [24].

The comparative C_5^+ selectivity and CH_4 selectivity for the C_1, C_2, C_3, and C_4 catalysts show that the catalyst prepared by the sol-gel technique has higher C_5^+ selectivity and lower CH_4 selectivity than the C_4 catalysts. The uniformity of the particle size improved the hydrogenation of carbon monoxide, and also it can be related to wall electron deficiency inside the CNT, which enhances the CO chemisorption, enlarges the residence time of the reactants, thus allowing more probability of longer carbon chains to be formed, which in turn increased the selectivity for C_5^+ products [21-25]. The decrease in the selectivity of CH_4 can be explained by the effective participation of olefins in the carbon-carbon chain propagation for the uniform cobalt clusters produced by sol-gel technique.

The chain length distribution of Fischer-Tropsch products formed on CNT supported cobalt catalysts can be well characterized by two ASF distributions. In all cases, a double-α-ASF distribution was required to fit data. Chain length distributions on C_1, C_2, C_3 and C_4 catalysts were calculated according to method presented by Nakhaei Pour et al. [34] and presented in Fig. 8. The trend lines are plotted for C_3^+ products to determine the chain growth probability, α. The chain growth probability was 0.81, 0.82, 0.84 and 0.86 for C_1, C_2, C_3 and C_4 catalysts, respectively. These results show that with increasing the cobalt cluster size, there is a shift in hydrocarbons to higher molecular weights. It seems that the steric hindrance for dissociative adsorption of CO and -CH2- monomer and addition of this monomer to the growing chain is better in the larger cobalt clusters [10]. According to Fig. 8, the catalyst prepared by the impregnation method (C_4) showed better selectivity for heavier hydrocarbon molecules (C_{10}^+), which can be explained by the presence of larger cobalt particle sizes (10^+ nm) than the catalyst prepared by sol-gel method. Large particles (10^+ nm) have high potential of re-adsorption and polymer chain initiation on the catalyst's surface [10,35].

According to Fig. 9 the olefin/paraffin mass ratio for the calcined C_1-C_3 catalysts decreases from 0.67 to 0.55 with increasing the particle size. Therefore, the slight decreasing might be related to the effective participation of olefins in the carbon-carbon chain propaga-

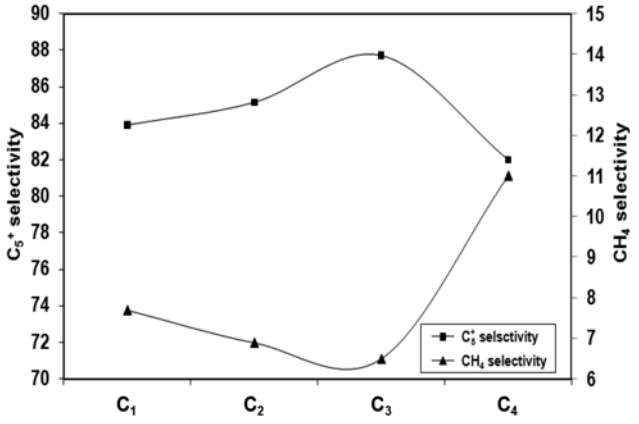

Fig. 7. C_5^+ and CH_4 selectivity of the calcined C_1-C_4 catalysts.

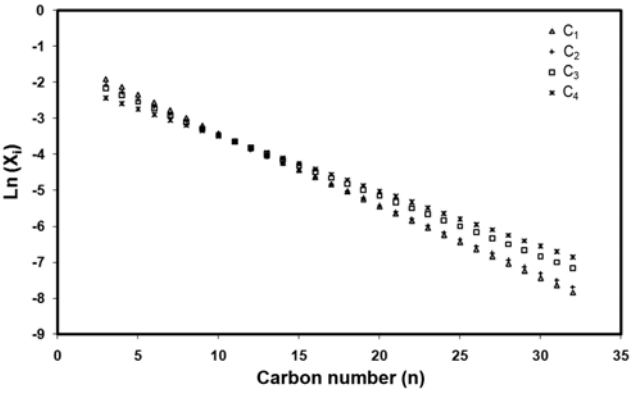

Fig. 8. Chain length distribution over C_1-C_4 catalysts, T=220 °C, H_2/CO=2, P=2.5 MPa, X_i mole fraction of component i.

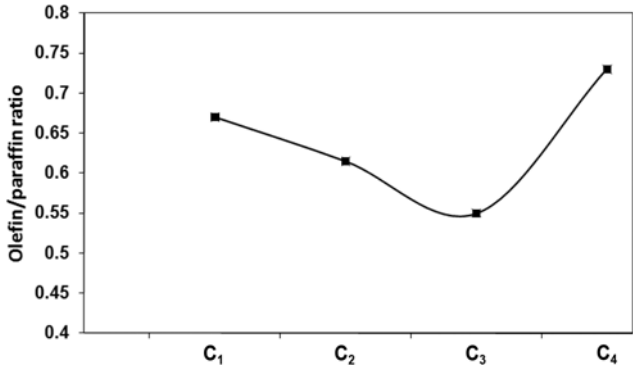

Fig. 9. Olefin/paraffin mass ratio for the calcined C_1-C_4 catalysts.

tion for larger cobalt cluster size, which enhanced the C_5^+ selectivity as mentioned above.

The olefin/paraffin ratio is higher for the C_4 catalyst compare to C_1-C_3 catalysts. It can be explained by the effective participation of olefins in the carbon-carbon chain propagation for the uniform cobalt clusters produced by sol-gel technique. On C_1-C_3 catalysts, α-olefins of the type R-CH=CH_2 can compete with carbon monoxide and heavier olefins for readsorption and chain initiation up to chain lengths C_{11}. The higher H_2 chemisorption on the C_1-C_3 catalysts means higher probability of CHx+H reactions, which consequently leads to a higher termination rate after C_{11} hydrocarbon chains (as shown in Fig. 8). So it should be mentioned that the measurements for α-olefin/n-paraffin ratios were taken for C_2-C_{11} hydrocarbons in this work. The shift towards olefin production over C_4 could also indicate lower hydrogenation activities for particles outside the CNT tubes (larger particles) than the particles inside the tubes [10].

In comparing our results with Bezemer et al. [1], compatibility is found between those results and our results in trend followed by catalysts C_4 and C_3 with respect to particle size, but mostly it must be attributed to lower hydrogenation activities for particles outside the CNT than the particles inside the tubes [10]. Catalysts supported with carbon nanofiber, morphologically differ from catalysts supported on CNT, which active phase positions mostly inside the tube according to our preparation procedure. In comparative study of olefin/paraffin ratio in catalyst supported CNT with particle size <9 nm and trend were followed by catalysts C_1-C_3, we must consider two parameters: first the particle size, and the second the confinement of active phase inside the tube, because it is more important the particle size effect for olefin/paraffin ratio and consequently on the FTS activity [10].

With above description we can conclude that our results are in good agreement with results published by Dalai et al. [10].

CONCLUSIONS

This research has been carried out using functionalized CNT supported cobalt catalysts to compare the effects of sol-gel technique for catalyst preparation with the common incipient wetness impregnation method at relatively high cobalt loadings (15 wt%). According to TEM analysis, cobalt nanoparticles produced with this special sol-gel technique show a narrow particle size distribution. As shown in TEM images, small Co particles (2-8 nm) are mostly confined inside the functionalized CNT, which in turn leads to a better interaction with the intern electron deficient walls of the CNT and favors the reduction of Co_3O_4 species. TPR results show the deposition of cobalt nanoparticles (synthesized by sol-gel technique) on the functionalized CNT, shifting the reduction steps to a lower temperature compared to the catalyst prepared by common impregnation method. Also, these results show that the metal-support interaction increases as the particle size decreases.

Functionalized CNT as a catalyst support of Co nanoparticles maintains high dispersion and reducibility of Co, which can be attributed to hydrogen spill-over effect of functional groups on CNT surface. This event will not normally occur in catalyst prepared by common impregnation method or with small particles supported on oxidic carriers. It was also found that FTS activity and selectivity of the catalysts is strongly dependent on the size distribution of the cobalt cluster. However, the particle's confinement within functionalized CNT may be more important than the particle size effect for the CO conversion and FTS activity and selectivity. Thus, improvement of the uniformity of the catalyst particles supported on functionalized CNT by proposed sol-gel technique leads to a better CO conversion, FTS activity, C_5^+ selectivity, stability of the products, and lower CH_4 selectivity, compared to that prepared by common incipient wetness impregnation. This new catalyst preparation method may offer an attractive alternative for nanoparticle synthesis with uniform and various sized distributions for fundamental catalytic studies, especially such for structure-sensitive FT catalysis.

ACKNOWLEDGEMENTS

Dr. Ali Nakhaeipour and Dr. Ahmad Tavassoli are acknowledged for their assistance. The authors are thankful to the Research Council of the Research Institute of the Petroleum Industry and to the Research and Development of the National Iranian Oil Company for their support of this work.

REFERENCES

1. G. L. Bezemer, J. H. Bitter, H. P. C. E. Kuipers, H. Oosterbeek, J. E. Holewijin, X. Xu, F. Kapteijn, A. J. van Dillen and K. P. de Jong, *J. Am. Chem. Soc.*, **128**, 3956 (2006).
2. A. Tavasoli, R. M. Malek Abbaslou, M. Trépanier and A. K. Dalai, *Appl. Catal. A*, **345**, 134 (2008).
3. J. Li, G. Jacobs, Y. Zhang, T. Das and B. H. Davis, *Appl. Catal. A*, **223**, 195 (2002).
4. M. E. Dry, *J. Chem. Technol. Biotechnol*., **77**, 43 (2001).
5. G. Jacobs, T. K. Das, Y. Zhang, J. Li, G. Racoillet and B. H. Davis, *Appl. Catal. A*, **233**, 263 (2002).
6. A. Martinez and G. Prieto, *J. Catal*., **245**, 470 (2007).
7. A. Tavasoli, Y. Mortazavi, A. A. Khodadadi, M. A. Mousavian, K. Sadagiani and A. Karimi, *Iranian J. Chem. Chem. Eng*., **35**, 9 (2005).
8. N. Koizumi, T. Mochizuki and M. Yamada, *Catal. Today*, **141**, 34 (2009).
9. P. Serp, M. Corrias and P. Kalck, *Appl. Catal. A.: Gen.*, **253**, 337 (2003).
10. M. Trépanier, A. K. Dalai and N. Abatzoglou, *Appl. Catal. A: Gen.*, **374**, 79 (2010).
11. A. Karimi, A. Nakhaei Pour, F. Torabi, B. Hatami, M. Alaei and M.

Irani, *J. Nat. Gas Chem*., **19**, 503 (2010).
12. M. Ojeda, S. Rojas, M. boutonnet, F. J. Perez-Alonso, F. Javier Garcia-Garcia and J. L. G. Fierro, *Appl. Catal. A*, **274**, 33 (2004).
13. Y. F. Zhang, J. X. Zhang, M. L. Qing and Q. Y. Zhang, *Mater. Lett*., **60**, 2443 (2006).
14. K. Soongprasit, D. Aht-Ong, V. Sricharoenchaikul and D. Atong, *Mat. Sci. Forum*, **658**, 29 (2010).
15. D. J. Lensveld, J. Gerbrand Mesu, A. J. van Dillen and K. P. de Jong, *Micropor. Mesopor. Mater*., **44-45**, 401 (2001).
16. A. J. van Dillen, R. J. A. M. Terörde, D. J. Lensveld, J. W. Geus and K. P. de Jong, *J. Catal*., **216**, 257 (2003).
17. J. van de Loosdrecht, M. van der Haar, A. M. van der Kraan, A. J. van Dillen and J. W. Geus, *Appl. Catal. A: Gen.*, **150**, 365 (1997).
18. B. Ernst, S. Libs, P. Chaumette and A. Kiennermann, *Appl. Catal. A*, **186**, 145 (1999).
19. A. Tavasoli, A. Karimi, Y. Mortazavi and A. Khodadadi, *Iranian J. Chem. Chem. Eng*., **36**, 25 (2005).
20. G. L. Bezemer, P. B. Radstake, V. Koot, A. J. van Dillen, J. W. Geus and K. P. de Jong, *J. Catal*., **237**, 291 (2006).
21. A. Tavasoli, K. Sadagiani, F. Khorashe, A. A. Seifkordi, A. A. Rohani and A. Nakhaeipour, *Fuel Proc. Technol*., **9**, 491 (2008).
22. M. Trépanier, A. Tavasoli, A. K. Dalai and N. Abatzoglou, *Fuel Proc. Technol*., **90**, 367 (2009).
23. M. Trépanier, A. Tavasoli, A. K. Dalai and N. Abatzoglou, *Appl. Catal. A*, **353**, 193 (2009).
24. A. M. Rashidi, A. Karimi, H. R. Bozorgzadeh, K. Kashefi and M. Zare, *J. Nat. Gas Chem*., **19**, 548 (2010).
25. W. Chen, Z. Fan, X. Pan and X. Bao, *J. Am. Chem. Soc*., **130**, 9414 (2008).
26. A. M. Rashidi, A. Nouralishahi, A. A. Khodadadi, Y. Mortazavi, A. Karimi and K. Kashefi, *Int. J. Hydrog. Energy*, **35**, 9489 (2010).
27. G. L. Bezemer, A. van laak, A. J. van Dillen and K. P. de Jong, *Stud. Surf. Sci. Catal*., **147**, 259 (2004).
28. Y. Zhang, Y. Liu, G. Yang, Y. Endo and N. Tsubaki, *Catal. Today*, **142**, 85 (2009).
29. H. Naeimi, A. Mohajeri, L. Moradi and A. M. Rashidi, *Appl. Surf. Sci*., **256**, 631 (2009).
30. R. Bechera, D. Balloy and D. Vanhove, *Appl. Catal. A*, **207**, 343 (2001).
31. G. P. Huffman, N. Shah, J. Zhao, F. E. Huggins, T. E. Hoost, S. Halvorsen and J. G. Goodwin, *J. Catal*., **151**, 17 (1994).
32. H.-Y. Lin and Y.-W. Chen, *Mater. Chem. Phys*., **85**, 171 (2004).
33. A. Martinez, C. Lopez, F. Marquèz and I. Diaz, *J. Catal*., **220**, 486 (2003).
34. A. Nakhaei Pour, Y. Zamani, A. Tavasoli, S. M. Kamali Shahri and S. A. Taheri, *Fuel*, **87**, 2004 (2008).
35. R. J. Madon and E. Iglesia, *J. Catal*., **139**, 576 (1993).